A factorial analysis of the marine carbon cycle and ocean circulation controls on atmospheric CO$_2$

David R. Cameron,[1] Timothy M. Lenton,[2] Andy J. Ridgwell,[3] John G. Shepherd,[4] Robert Marsh,[4] and Andrew Yool[4]

[1] A factorial experiment with a new Earth system model of intermediate complexity is used to assess the sensitivity of atmospheric CO$_2$ to organic, carbonate and solubility pumps, ocean circulation state, and climate feedback. An analysis of variance of the results reveals that the organic, carbonate, and solubility pumps act multiplicatively and account for 94% of the variance of atmospheric CO$_2$. The organic pump explains 63% (89 ppm), the solubility pump 24% (55 ppm), the carbonate pump 6% (28 ppm), and ocean circulation 0.3% (12 ppm) of the variance. Removing all pumps increases atmospheric CO$_2$ from 278 to 525 ppm. Including interactions with all the pumps increases the effects of ocean circulation from 12 to 56 ppm. However, the ocean circulation states used are unlikely to span the full range of possible states. Changes in Pacific circulation have more effect on atmospheric CO$_2$ than Atlantic circulation.

1. Introduction

[2] Interacting physical, chemical and biological processes in the ocean play a key role in regulating atmospheric CO$_2$. The responsible processes can be thought of in terms of three "pumps" of carbon operating in the ocean: the solubility pump, the organic (or soft tissue) pump, and the carbonate pump (also known as the alkalinity, hard tissue or "counter" pump, because it exerts an opposite effect on atmospheric CO$_2$ to the organic pump) [*Volk and Hoffert*, 1985]. Their absolute and relative strengths and net impact on atmospheric CO$_2$ should depend on the circulation state of the ocean, while further modulation of CO$_2$ is expected to occur through feedback of atmospheric CO$_2$ on radiative forcing, sea-surface temperature and hence on the ocean surface chemistry and circulation.

[3] There is a relatively long history of model assessments of the effect of different ocean carbon pumps on atmospheric CO$_2$. This began with relatively simple "box" model representations of ocean circulation with often idealized biogeochemical processes [*Broecker and Peng*, 1986; *Volk and Hoffert*, 1985]. Increasingly, Ocean General Circulation Models (OGCMs) and intermediate complexity models are being used, to assess how the marine carbon cycle contributes to or is affected by global change [*Archer et al.*, 2000b; *Bopp et al.*, 2001, 2003; *Sarmiento and Le Quere*, 1996; *Sarmiento et al.*, 1998; *Joos et al.*, 1999; *Plattner et al.*, 2001], and to assess the factors that might account for glacial CO$_2$ drawdown [*Archer et al.*, 2000a].

[4] The different types of ocean model appear to have quite different weightings of the processes setting equilibrium atmospheric CO$_2$ [*Broecker et al.*, 1999; *Archer et al.*, 2000a]. In the so-called "Harvardton-Bear" box models [*Knox and McElroy*, 1984; *Sarmiento and Toggweiler*, 1984; *Siegenhaler and Wenk*, 1984], cold high-latitude surface waters, that are in direct contact with the deep ocean, dictate the CO$_2$ of the atmosphere and thus the warm surface ocean. OGCMs are generally much less high-latitude sensitive than the box models, although there is considerable spread between different OGCMs and some prove even more high latitude sensitive than box models [*Archer et al.*, 2000a]. The reason for this is a subject of active debate. *Archer et al.* [2000a] attribute it to high vertical diffusivity, while *Broecker et al.* [1999] claim that a greater exchange of CO$_2$ between warm surface waters and the cold deep water in OGCMs is responsible. In contrast, *Toggweiler et al.* [2003a, 2003b] proposed that it is excessive disequilibrium between high-latitude surface waters and the atmosphere in one OGCM that makes it less high-latitude sensitive compared to observations, while box models may have too little disequilibrium related to a convective control identified by

[1]Centre for Ecology and Hydrology, Bush Estate, Penicuik, UK.
[2]School of Environmental Sciences, University of East Anglia, Norwich, UK.
[3]Department of Earth and Ocean Sciences, University of British Columbia, Vancouver, British Columbia, Canada.
[4]National Oceanography Centre, Southampton, UK.

Table 1. Key Model Parameters[a]

Parameter	Standard Model Value
Ocean isopycnal diffusivity	4126.354 m^2 s^{-1}
Ocean diapycnal diffusivity	2.048 $\times$ 10^{-5} m^2 s^{-1}
Ocean drag	3.433 day^{-1}
Ocean wind stress scale	1.667
Sea ice diffusivity	6249.426 m^2 s^{-1}
EMBM heat diffusivity	375,4760. m^2 s^{-1}
EMBM moisture diffusivity	1,753,441.596 m^2 s^{-1}
EMBM heat advection ratio	6.036 $\times$ 10^{-2} (zonally)
	0.0 (meridionally)
EMBM moisture advection ratio	0.137 (zonally)
	0.126 (meridionally)
T diffusion width	1.3 radians
log$_{10}$(T diffusion slope/0.1)	0.16
FW adj	0.29 Sv

[a]See *Edwards and Marsh* [2005] for a discussion of each parameterization.

Ridgwell [2001]. This disagreement between models needs to be resolved, because understanding the main oceanic carbon sinks and their relative importance is crucial for our ability to predict future climate change.

[5] Existing studies assume as a starting point either a modern circulation state of the ocean or a modified Atlantic circulation more appropriate for the Last Glacial Maximum. The limitation of contrasting the modern system with only a single alternative circulation state is that the sensitivity of atmospheric CO$_2$ to other aspects of assumed or modeled ocean circulation may be missed. We address this by considering fundamental reorganizations (''modes'') of ocean circulation, and ask how the relative strengths of the solubility pump, organic pump, and carbonate pump depend on the mode of ocean circulation, and how the nonlinear combination of these factors affects atmospheric CO$_2$. To do this we designed a factorial experiment with an Earth system model of intermediate complexity (EMIC) (section 2) that can capture all of the factors and their interactions. We are able to adjust the parameterization of our model such that we can mimic different types of model. By using the same model we avoid the uncertainties of interpretation involved in comparing results from different models. Additional information is available in the auxiliary material[1].

2. Model

[6] As part of the Grid ENabled Integrated Earth system model (GENIE) project (www.genie.ac.uk), a representation of the marine carbon cycle, BIOGEM, was coupled to an ocean-atmosphere-sea ice climate model, C-GOLDSTEIN [*Edwards and Marsh*, 2005]. The resulting model is the first step toward a more complete Earth system termed ''GENIE-1'' and we use that shorthand to describe the model here. It can perform 1000 years of simulation in 1 hour on a standard PC making it an ideal tool for a factorial experiment where many model simulations of thousands of years are required to capture the equilibrium state and the full factorial design. The standard configu-

ration of GENIE-1 has a modern-day thermohaline circulation and ocean biogeochemistry.

2.1. Climate Model

[7] C-GOLDSTEIN comprises a reduced physics (frictional geostrophic) 3D ocean model coupled to a 2D energy-moisture balance model (EMBM) of the atmosphere and a dynamic-thermodynamic sea-ice model. The ocean model includes realistic bathymetry, an isoneutral and eddy-induced mixing scheme and spatially varying drag. The model is configured on a 36 $\times$ 36 equal-area grid, with eight logarithmically spaced depth levels in the ocean. In the work here, we use a nonseasonal version of the model (annual average insolation). See *Edwards and Marsh* [2005] for a full description of the model and its base parameterization.

[8] We base the physical state of our standard configuration of GENIE-1 on a study in which its key physical parameters have been tuned using an Ensemble Kalman Filter with ocean and surface atmospheric data in order to best reproduce the current ocean circulation state and surface climate [*Annan et al.*, 2004; *Hargreaves et al.*, 2004]. We set each key parameter of the model (Table 1) to the mean value of the 54-member tuned ensemble from *Hargreaves et al.* [2004]. The resulting ''ensemble mean'' model sits in the mid-range of responses of the full ensemble, and reproduces the physical state of the present-day ocean comparably well to the best of the models tested in the Ocean Carbon-Cycle Model Intercomparison Project (OCMIP) [*Orr et al.*, 2001; *Hargreaves et al.*, 2004]. The resulting physical ocean state is termed in this study the ''normal conveyor'' and is shown at the top of Figure 1 for the Atlantic and Pacific oceans.

2.2. Marine Carbon Cycle Model

[9] The marine carbon cycle (BIOGEochemical Model, ''BIOGEM'') component of GENIE-1 is based on a single nutrient (PO$_4$) representation of ocean biogeochemical cycling. BIOGEM vertically redistributes, according to processes of biological uptake, particulate matter remineralization and air-sea gas exchange, a set of geochemical tracers advected online within the model ocean. In this initial version of GENIE-1 these tracers are carbon (DIC), alkalinity (ALK) and phosphate (PO$_4$) (in addition to temperature and salinity). The biogeochemical scheme is similar to that used in many other marine carbon cycle models [*Broecker and Peng*, 1986; *Plattner et al.*, 2001; *Sarmiento et al.*, 1998] and follows *Ridgwell* [2001] and *Ridgwell et al.* [2002] unless otherwise stated. Nutrients, together with dissolved inorganic carbon (DIC), are taken out of solution in the sunlit surface ocean layer through biological action and exported in particulate form (as particulate organic matter, POM) to deeper layers. As it settles through the water column, POM is subject to remineralization processes (primarily bacterial metabolism), resulting in the release of dissolved constituent species. The process of remineralization in the ocean is implemented according to a predetermined profile of relative sinking flux. Associated with the biological fixation of carbon is the formation of CaCO$_3$ and further removal of DIC in addition to ALK. CaCO$_3$ is similarly

---

[1]Auxiliary material is available at ftp://ftp.agu.org/apend/gb/2005GB002489.
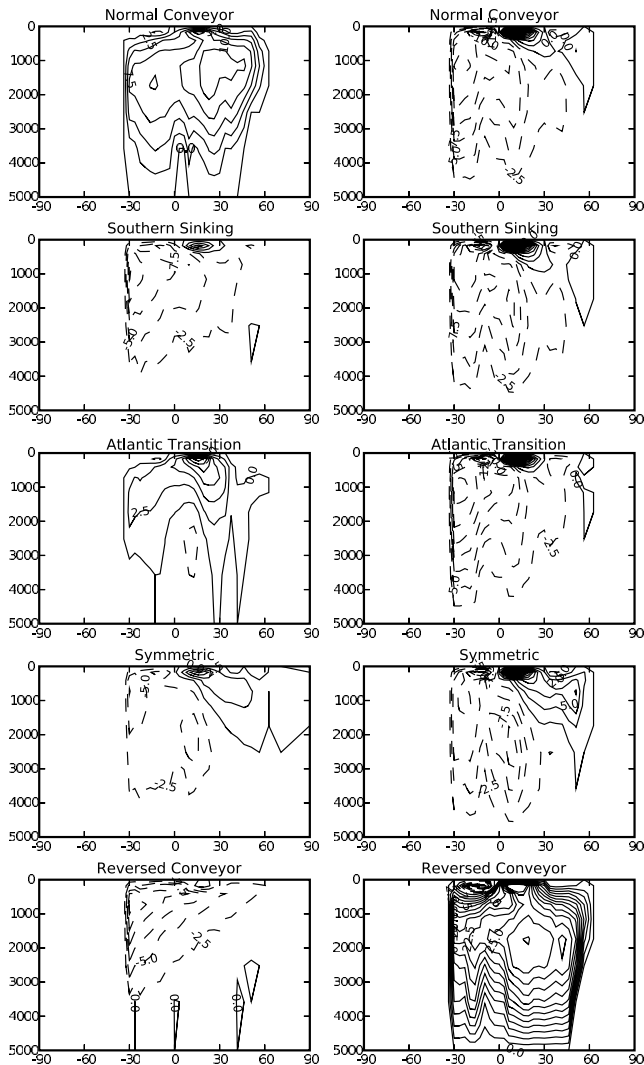
Figure 1. (left) Atlantic and (right) Pacific zonal mean overturning circulation for the five circulation states. The vertical axis is ocean depth in kilometers and the horizontal axis is latitude. The units are Sverdrups.

dissolved in the water column following a prescribed remineralization profile. CO$_2$ is exchanged with a well-mixed atmosphere across the air-sea interface and the value of atmospheric CO$_2$ predicted by BIOGEM is used as input to the radiative scheme of the atmospheric model, thus providing climate feedback. All particulate material (POM and CaCO$_3$) reaching the sediment surface is instantaneously remineralized and the dissolved constituents returned to the overlying ocean cell.

[10] The component parameterizations specific to the version of BIOGEM used here are as follows.

[11] 1. Phosphate concentrations in each surface ocean cell are restored with a characteristic time constant toward a prescribed target concentration. Excess PO$_4$ removed is converted into organic matter, while any deficit of model PO$_4$ compared to the target is left unchanged. The particulate organic phosphate is exported out of the surface layer, taking carbon with it from solution in a "Redfield" ratio of

1:106 [*Redfield et al.*, 1963]. In this study we chose to restore surface phosphate toward zero, so that the effects on the organic and carbonate pumps of changes in circulation state would be captured in a consistent way. In contrast, a methodology of restoring to present-day observations [*Gnanadesikan et al.*, 2002] requires that ocean circulation does not change significantly, a criteria that we violate by testing radically different circulation states. A restoration timescale of 6 years was found to give results which compare reasonably with observational data (Figures 2 and 3) and to best mimic the effect of restoring phosphate rapidly (0.1-year timescale) toward present-day observations [*Gnanadesikan et al.*, 2002]. A timescale of 6 years is much longer than the time-scale of nutrient uptake by phytoplankton; instead it represents the timescale for export of particulate matter from the euphotic zone and thus implicitly includes the effects of both the recycling of POM within the surface ocean and of the production and recycling of dissolved organic matter.

[12] 2. A double exponential formulation [*Andersson et al.*, 2004] is used to partition down through the water column the solute release arising from the remineralization of particulate matter. We chose e-folding depths for the two organic matter fractions of 250 m and 5000 m, with an initial 0.85:0.15 split between them. Although these length scales are somewhat longer than those diagnosed by *Andersson et al.* [2004] from deep ocean respiration patterns we find that they enable a reasonable interior ocean PO$_4$ (Figure 3) field to be produced. Our choice also allows the *Martin et al.* [1987] curve to be approximated at relatively shallow depths while at the same time retaining
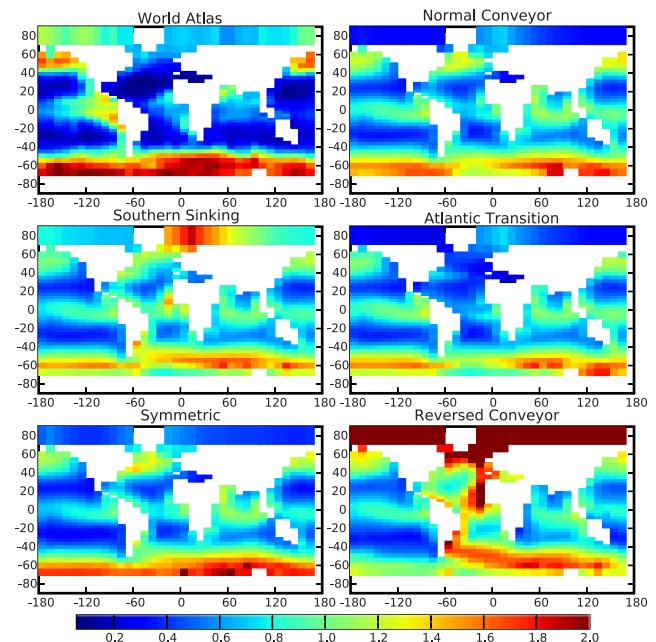
Figure 2. Comparison of annual mean surface phosphate for the Levitus World Ocean Atlas (transformed to the model grid) with the five circulation states. The units are μmol kg^{-1}.
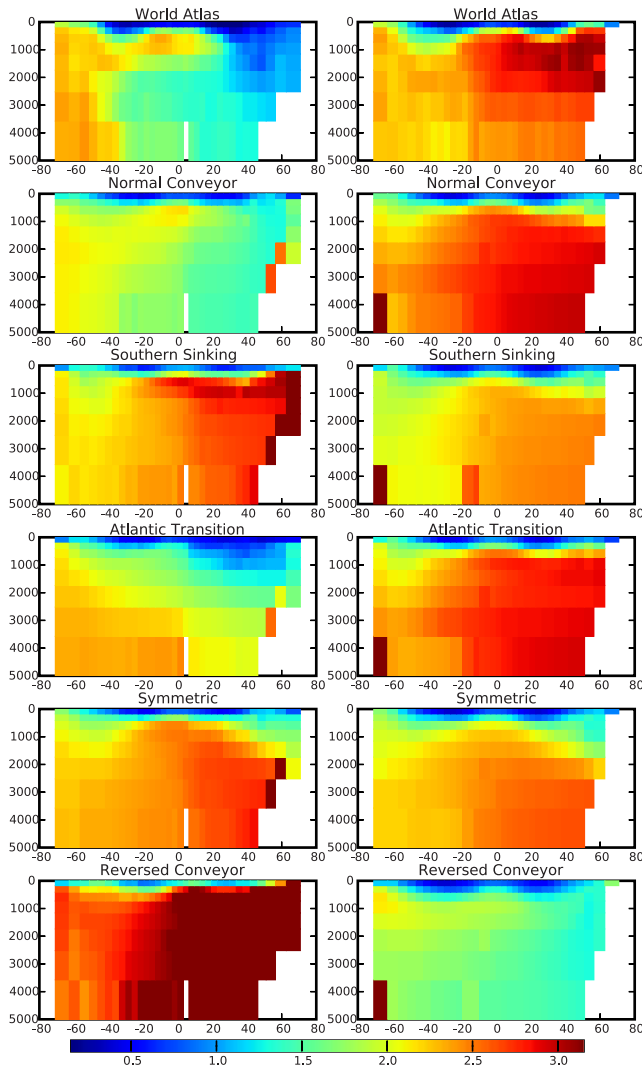
Figure 3. Comparison of (left) Atlantic and (right) Pacific zonal annual mean phosphate for the Levitus World Ocean Atlas (transformed to the model grid) with the five circulation states. The units are μmol kg^{-1}.

a significant residual flux fraction at depth [*Ridgwell*, 2001].

[13] 3. A double exponential formulation is also used to remineralize CaCO$_3$ in the water column, with the two e-folding depths (500 m and ∞ m) and initial partitioning between them (0.6:0.4) following *Ridgwell et al.* [2002].

[14] 4. A uniform air-sea CO$_2$ transfer coefficient of 0.061 mol m^{-2} μatm^{-1} yr^{-1} is employed [*Maier-Reimer*, 1993] to exchange CO$_2$ with a well-mixed atmosphere.

[15] With this standard configuration we obtain a global total export flux of particulate organic matter below the uppermost 175-m-thick surface layer of the ocean model of 11.2 GtC yr^{-1}, which is at the upper end of the range of 7.5–11.0 GtC yr^{-1} predicted by other 3D ocean carbon cycle models [*Archer et al.*, 2000a; *Heinze et al.*, 1999; *Six and Maier-Reimer*, 1996]. Although we thus achieve first-order success in representing the marine carbon cycle with

this basic single-nutrient scheme, the lack of seasonality and additional nutrients (such as Fe) in this particular version of BIOGEM results in a slight overestimate of phosphate values in the oceanic gyres and underestimated values in the Southern Ocean, equatorial Pacific, and North Pacific, the classic iron-limited high-nutrient low-chlorophyll (HNLC) regions [*Watson*, 2001]. The requirement that PO$_4$ concentrations must be kept relatively high in HNLC regions (particularly the Southern Ocean), in the absence of explicit representation of Fe limitation or a seasonal mixed layer depth, also contributes to the apparently long characteristic uptake-export time constant.

[16] For representing the marine carbon cycle, OGCM-based model studies often employ a temperature and/or H$_4$SiO$_4$ availability dependant parameterization of the ratio of CaCO$_3$ to Organic-C in the export flux sinking from the top layer of the ocean [*Archer et al.*, 2000b; *Heinze et al.*, 1999; *Maier-Reimer*, 1993]. However, to simplify the interpretation of the factorial experiment we chose a uniform CaCO$_3$:POC rain ratio value of 0.2 as default here, consistent with the mean global export ratio of the Hamburg LSG OGCM model and its variants [*Archer et al.*, 1998, 2000b; *Heinze et al.*, 1999]. We note that although recent studies have suggested that the global average CaCO$_3$:POC may be considerably lower than this, perhaps as low as 0.06–0.08 [*Yamanaka and Tajika*, 1996; *Sarmiento et al.*, 2002], the question is not yet resolved.

[17] Having set the strength of the organic and carbonate pumps, we ran GENIE-1 to equilibrium with the atmospheric CO$_2$ restored to the preindustrial value of 278 μatm. This resulted in a mean ocean DIC concentration of 2214 μmol kg^{-1}, a value slightly lower than the value of $\approx$2235 μmol kg^{-1} required in some other preindustrially configured marine carbon cycle models [*Yamanaka and Tajika*, 1996]. Along with the mean oceanic alkalinity (ALK) and PO$_4$ of 2374 μmol eq kg^{-1} and 2.22 μmol kg^{-1}, respectively, the diagnosed value of DIC was used as an initial value for the subsequent simulations in this paper.

3. Intermodel Comparison Tests

[18] Before considering the sensitivity of the ocean carbon cycle to fundamental changes in the model of ocean circulation, we first place the characteristics of the GENIE-1 marine carbon cycle in the context of other ocean biogeochemical models by performing the comparison tests proposed by *Broecker et al.* [1999], *Archer et al.* [2000a], and *Toggweiler et al.* [2003a, 2003b].

3.1. HBEI Test

[19] First we calculated the Harvardton-Bear equilibrium index (HBEI) [see *Broecker et al.*, 1999, equation (4)]. This is done by perturbing the ocean surface solubility coefficient between 40°N and 40°S and measuring the warm ocean surface pCO$_2$ immediately after the change and after the equilibrium state has been reestablished to form the index. Near zero values suggest that the high latitudes dominate whereas values closer to 1 suggest that the warm low latitudes are important in determining atmospheric CO$_2$. *Broecker et al.* [1999] found that three-box models tend to have low values (0.1–0.13), with multibox models having
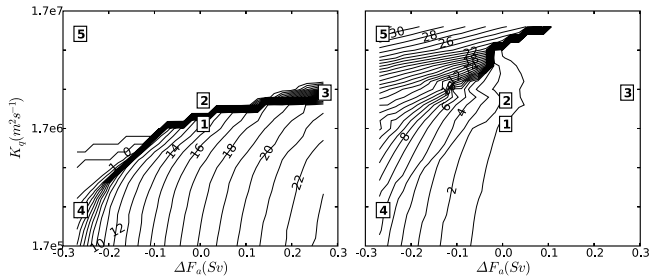
Figure 4. (left) Atlantic and (right) Pacific maximum overturning circulation (Sv) in (ΔF_a, K_q) parameter space where ΔF_a is the Atlantic to Pacific moisture flux in Sverdrups and K_q is atmospheric moisture diffusivity in m^{2}s^{-1}. The five chosen circulation states are marked by numbers in boxes (see section 4.1 for details).

slightly higher values (0.14–0.22) whereas GCMs have larger values still (Princeton model 0.24, Hamburg LSG OGCM 0.32). They attributed these results to a greater exchange between warm and cold waters of the ocean in GCMs than in box models. We found an HBEI value of 0.24 for GENIE-1. *Ridgwell* [2001] found that the HBEI index was sensitive to convection and suggested that differences between the seasonality of convection in the Princeton (annual average) and the Hamburg (seasonal) models may be important in accounting for their different HBEI values. It is interesting to note that GENIE-1 has an identical value to another annual average GCM (the Princeton model).

3.2. Archer Test

[20] The second test follows *Archer et al.* [2000a] who initialize ocean DIC to 2085 μmol kg^{-1} and switch off any biological processes in the ocean, recording atmospheric CO$_2$ once the model has come to an equilibrium state. In agreement with *Broecker et al.* [1999] and *Archer et al.* [2000a], we found that there was generally a significant difference in atmospheric CO$_2$ values for box models (typically 220–230 μatm) and depth coordinate GCMs (250–290 μatm, although the OM3 GCM with lateral diffusion oriented along isopycnal surfaces had low values somewhat similar to box models. Thus spurious mixing may be affecting the result for z-coordinate GCMs with diffusion along depth surfaces. The standard version of GENIE-1 used in the factorial experiment was found to give a surprisingly low value of 224 μatm.

[21] This was thought to be associated with an erroneously strong and deep-penetrating positive overturning cell in the Southern Ocean. By experimenting with key model parameters (halving the horizontal/isopycnal ocean diffusivity and increasing the vertical/diapycnal diffusivity by an order of magnitude) the value obtained increases to 237 μatm. This value is increased further to 241 μatm if the Atlantic to Pacific moisture flux (ΔF_a) is increased to the largest value used in the factorial experiment (see section 4.1 and Figure 4). These changes to the model parameters affected the positive overturning cell in the Southern Ocean making it weaker and shallower (not shown).

[22] Thus these sensitivity analyses with different model parameters and ocean circulation demonstrate that with a range of values of 224 to 241 μatm, GENIE-1 consistently falls significantly lower than z-coordinate GCMs (250 to 290 μatm), but higher than isopycnic GCMs (210 to 220 μatm) and slightly higher than "box" models (220 to 230 μatm) [*Archer et al.*, 2000a].

3.3. Toggweiler Test

[23] The final test follows *Toggweiler et al.* [2003a, 2003b] and diagnoses the influence of model air-sea disequilibrium on the solubility and organic ocean carbon pumps. The carbon pumps are isolated using the approach described in section 4.1. For this test, *Toggweiler et al.* [2003a, 2003b] fix atmospheric pCO$_2$ to a pre-industrial value of 278 ppm and compare the surface to deep DIC difference for model simulations where they increase the piston velocity or air-sea gas coefficient, such that the atmosphere and surface ocean are forced to be in close equilibrium, with one where the air-sea coefficient is unaltered. They show that the OGCM (POBM) has greater air-sea disequilibrium than box models. This has the effect of increasing the relative strength of the organic pump and decreasing the relative strength of the solubility pump, in the OGCM. The differences in the surface to deep DIC for models with normal and fast gas exchange for GENIE-1 are found to be −35 and 30 μmol kg^{-1} for the solubility and organic pumps respectively. Comparing these results with Figure 3 of *Toggweiler et al.* [2003a] and Figure 3 of *Toggweiler et al.* [2003b] for the GCM and with the values obtained for the box models we find that, consistent with the Archer test above, GENIE-1 lies in between the GCM (−70 and 50 μmol kg^{-1}) and the box model (−24 and 29 μmol kg^{-1}), with values closer to the box model.

4. Method

4.1. Factorial Experiment Design

[24] The different circulation states used in the factorial analysis were identified from an ensemble experiment [*Marsh et al.*, 2004] in which two parameters were varied: (1) atmospheric freshwater transport from the Atlantic to the Pacific, ΔF_a, and (2) atmospheric moisture diffusivity, K_q, which primarily influences equator-pole freshwater transport (see *Marsh et al.* [2004] for further details). The default settings of ΔF_a and K_q were taken as the center point of the parameter space (normal conveyor-state 1). ΔF_a was varied by ±≈0.3 Sv which takes the Atlantic to Pacific moisture flux from near zero to twice its default value. K_q was varied by an order of magnitude increase or decrease. In total there were 29 × 31 separate runs of the model, each of which is run to equilibrium. The resulting maximum meridional overturning circulation (MOC) for each run is plotted on a ΔF_a-K_q parameter space (Figure 4). From the resulting parameter space, four further ΔF_a-K_q combinations were chosen that capture distinct circulation states (Figure 4 shows the five circulation states marked).

[25] The MOC for all five states are shown for the Atlantic and Pacific in Figure 1. The states can be summarized as follows:
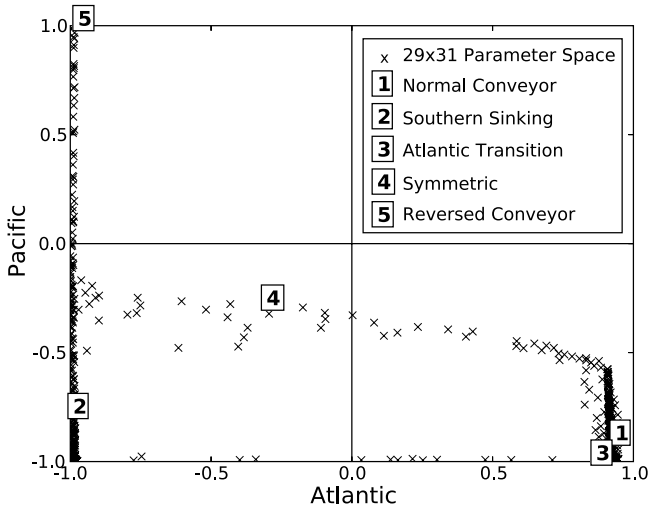
Figure 5. Circulation phase space representing the direction and degree of asymmetry between the Atlantic and Pacific ocean circulations (see equation (1) and section 4.1 for details). Each member of the 29 × 31 (ΔF_a, K_q) ensemble experiment is marked by a cross, and the five chosen circulation states (section 4.1) are also shown.

[26] 1. The normal conveyor approximates the present-day ocean circulation state; with a positive Atlantic and a negative Pacific meridional overturning circulation.

[27] 2. Southern sinking is just over the nearby "cliff edge" in ΔF_a-K_q parameter space [*Marsh et al.*, 2004], with the Atlantic circulation reversed and the Pacific circulation similar to the normal conveyor.

[28] 3. The Atlantic transition captures a region of parameter space where an intermediate strength positive Atlantic circulation is stable. It was picked from within a "transition" region of ΔF_a-K_q parameter space; that is where the circulation state is in transition from a strong cell of one sign to another.

[29] 4. The symmetric state captures a transition region for both the Atlantic and Pacific, where positive and negative cells for the Atlantic and Pacific are close to being equal and are weak.

[30] 5. The reversed conveyor marks the region of parameter space with a strong positive Pacific circulation and a negative Atlantic circulation.

[31] In addition to the parameter space diagrams (Figure 4), we adopted a useful diagnostic tool for characterizing structurally distinct ocean circulation states proposed by Shepherd and Hosoe [*Hosoe*, 2004]. All 29 × 31 members of the ΔF_a-K_q ensemble experiment are plotted in a circulation phase space representing the direction and degree of asymmetry of the maximum meridional stream functions for the Atlantic and Pacific (Figure 5), using pairs of values of an asymmetry metric,

$$X_{atlantic}, X_{pacific} = \frac{\Psi_+ + \Psi_-}{|\Psi_+| + |\Psi_-|}. \tag{1}$$

For each ocean basin (i.e., axis), the values 1 or −1 denote dominance by a single positive or negative cell (total

asymmetry), whereas 0 indicates there are positive and negative cells of equal strength (symmetry). Figure 5 shows that the ensemble members clump somewhat into four groupings with at least one of five chosen states in each of these main groupings. The first is a group where the Atlantic cell is strongly asymmetric and positive, and the Pacific cell is generally strongly asymmetric and negative; states 1 and 3 are members of this group. The second grouping has a Pacific cell of either sign and varying asymmetry and a strongly asymmetric negative Atlantic cell; states 5 and 2 belong to this group representing positive and negative Pacific cells, respectively. The third grouping has a strongly asymmetric negative Pacific cell and an Atlantic cell of either sign and varying asymmetry; state 3 is a member of this grouping. Finally, the fourth grouping is one where all the members have a weakly asymmetric Pacific cell and Atlantic cells of either sign and varying asymmetry; state 4 is a member of this group and is relatively close to symmetric for both the Pacific and the Atlantic. The first and second groups have by far the largest populations with the third and fourth groupings having a tiny number of members by comparison. It is interesting to note that there are no members which have a positive Atlantic cell and a positive Pacific cell and all members which have a positive Pacific cell also have a strongly asymmetric Atlantic cell. Both the parameter space diagram (Figure 4) and the phase space diagram (Figure 5) suggest that the five chosen states represent the main distinct equilibrium ocean circulation states in the two-parameter sweep of *Marsh et al.* [2004].

[32] For each of the five circulation states, our factorial experiment involved switching the following factors on or off.
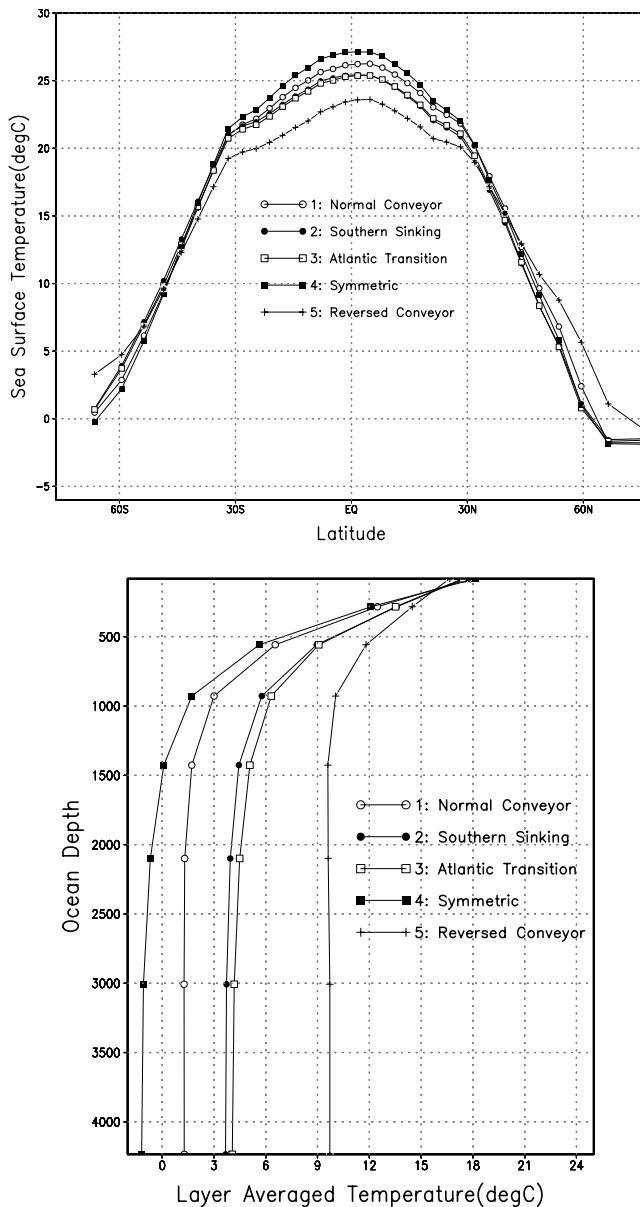
[33] 1. The organic (or soft tissue) pump (OrgC) is switched off by setting an extremely small P:C ratio. To leave the carbonate pump (CaCO$_3$) switched on, the CaCO$_3$:OrgC ratio was augmented to compensate for the smaller P:C so that P:CaCO$_3$ was unchanged.

[34] 2. The carbonate pump (CaCO$_3$) is switched off by setting the CaCO$_3$:OrgC ratio to zero.

[35] 3. The solubility pump (Sol) is switched off by feeding a uniform ocean temperature to the routine calculating the thermodynamic "constants" for surface water chemistry. The temperature used is the global average SST (Sea Surface Temperature) (289.68K), taken from a standard run of the model. The other circulation states used in this study were not found to have significantly different global average SSTs (Figure 6).

[36] 4. Climate feedback in the model can also be switched on or off. As described in section 2.2, the input value of CO$_2$ to the atmospheric radiation scheme is predicted by BIOGEM (the marine carbon cycle scheme) thus providing a climate feedback. This climate feedback can be switched off by using a default atmospheric pCO$_2$ of 278 ppm as input to the atmospheric radiation scheme.

[37] All factorial combinations of OrgC, CaCO$_3$, Sol and Clim were simulated for each of the five circulation states, which gives 80 model runs in total. Each integration lasted 5000 model years to ensure that the model had reached equilibrium. The ensemble of runs was done in

Figure 6. Zonal mean sea surface temperature (SST) and layer mean ocean temperature for the solubility pump only model (Sol: see section 4.1).

the use of a General Linear Model (GLM), for categorical variables (i.e., those which take only certain discrete values). Since this is a standard technique only a brief introduction will be given here, for more details see *Davies and Goldsmith* [1972]. The GLM framework also includes conventional regression analysis for continuous variables: an excellent account is given by *Grafen and Hails* [2002]. It is most commonly applied to the analysis of data from observations obtained from statistically designed experiments, but it is equally applicable to the analysis of model output, and the analysis of the results of multivariate sensitivity testing.

[39] ANOVA involves choosing a response (dependent) variable of interest, in this case atmospheric CO$_2$, and fitting a hierarchy of statistical models including and excluding the various factors (explanatory variables), separately and together, in order to determine how much of the total variance can be explained and the magnitude of the effects. The effects of the variables separately are known as main effects, those when they are fitted in combination are known as interactions. With a full factorial design (as in this case) all the interactions up to the highest order can be estimated, however the aim is to find a parsimonious model that can explain most of the variance with the minimum number of effects and interactions included. This parsimonious model determines which effects and interactions are significant.

[40] The main benefit of using the ANOVA technique is that it allows us to quantify the extent to which the different ocean circulations and pumps in isolation and together unambiguously account for the variation in atmospheric CO$_2$. The sum of the squares or variance given can be "normalized" by the degree of freedom of the effect in question. This gives a robust measure of the statistical significance of the effect and is termed the adjusted mean square. Both of these quantities are shown in Table 2. In addition to providing the fraction of the total CO$_2$ variance accounted for by the different factors and interactions, the technique also provides the magnitude of the estimated effects themselves in ppm, for atmospheric CO$_2$. This is similar to a regression coefficient and has also been included as part of the analysis and is given in Table 2.

[41] The ANOVA was undertaken on both CO$_2$ and log(CO$_2$) as the output variable, in order to ascertain

4.2. Analysis of Variance (ANOVA)

[38] The relatively complex setup of our experiment, involving 80 combinations of oceanic circulations, pumps and climate feedback, does not lend itself to an unambiguous interpretation of the factors affecting atmospheric CO$_2$. Therefore, to aid evaluating the effects of individual factors on atmospheric CO$_2$, the results were subjected to an Analysis of Variance (ANOVA). This is a special case of

parallel, using the Condor scheduler to submit the jobs, on a 120-processor Beowulf cluster at the Centre for Ecology and Hydrology, Edinburgh, thus taking only a few hours of elapsed time.

Table 2. ANOVA Table for Atmospheric pCO_2 Using a Parsimonious Model Where Factors and Interaction Terms With an Adjusted Mean Square Less Than 1000 are Discarded[a]

Source	DF	Seq SS	Adj MS	Maximum Effect, ppm
Circ	4	11613	2903	12.23
CaCO3	1	63164	63164	28.10
Sol	1	240674	240674	54.85
OrgC	1	638461	638461	89.33
Circ*Sol	4	27360	6840	24.28
Circ*OrgC	4	12717	3179	19.29
CaCO3*OrgC	1	2338	2338	5.41
Sol*OrgC	1	3800	3800	6.89
Error	62	3862	62	
Total	79	1003988		

[a]DF, degrees of freedom; Seq SS, sequential sum of squares; Adj MS, adjusted mean square.
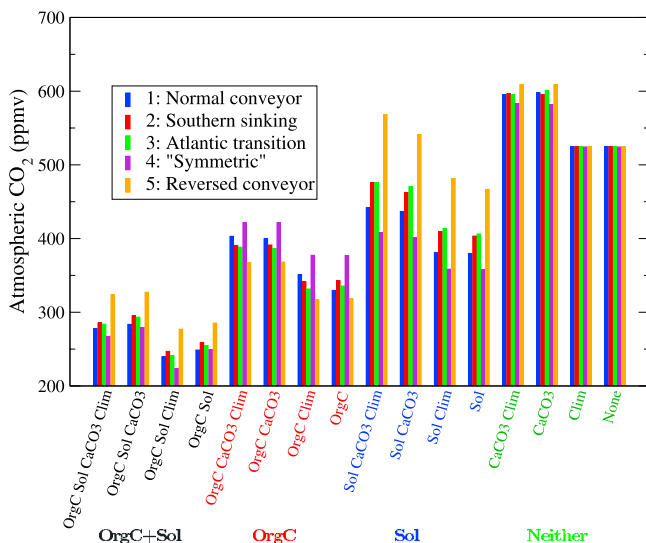
Figure 7. Results of the factorial experiment, showing equilibrium atmospheric CO$_2$ for the five circulation states and for each combination of factors. The factors are: OrgC, organic pump; Sol, solubility pump; CaCO3, carbonate pump; Clim, climate feedback. For a present-day ocean circulation state (state 1), there is a 250-ppm increase in CO$_2$ due to switching off all the pumps. The organic pump has the largest effect on CO$_2$ followed by the solubility and then the carbonate pump. Ocean circulation has a smaller but significant impact on the relative strength of the pumps, with the reversed and symmetric states having the largest impact. Climate feedback has the smallest effect on CO$_2$.

whether factors are best considered additive or multiplicative in their influence [*Grafen and Hails*, 2002]. log(CO$_2$) also gives a measure of the radiative impact on climate of a change in marine carbon cycling. Since the model results being analyzed are derived from a numerical experiment where there are no replicate samples and no sampling error, the estimates of test statistics obtained are only relative and indicative. We found an adequate and parsimonious model by discarding all factors (and interaction terms) as insignificant if they had an adjusted mean square of less then 1000, for the additive model and 0.002 for the multiplicative (log-transformed) model. This leaves us with a small residual error term due to the factors not fitted, but this cannot strictly be interpreted as a normal statistical error. These parsimonious models provide an excellent representation of the results, accounting for 99.62 and 99.64% of the variance, respectively.

5. Results and Discussion

[42] Figure 7 shows atmospheric CO$_2$ versus the factors that have been varied in this study. For a thermohaline circulation state like that of the present day (state 1), there is a 247 ppm increase (from 278 to 525 ppm) in atmospheric CO$_2$ due to switching off the organic, carbonate and solubility pumps.

[43] The factor having the largest single impact on CO$_2$ is the organic pump, next comes the solubility pump, then the carbonate pump. The ocean circulation state has a significant impact on the relative strength of the different pumps, especially for circulation states 4 and 5.

[44] In addition to estimating the magnitudes of the changes in CO$_2$ due to switching on and off the various factors (Figure 7) we can unambiguously isolate the sensitivity of atmospheric CO$_2$ to the various factors and their interactions using the parsimonious ANOVA. The results for atmospheric CO$_2$ are given in Table 2. In addition to the percentages of the adjusted mean square given by the main effects and their interactions we also report the maximum magnitude (in ppm) of the effects themselves in brackets (section 4.2). Without the ANOVA we have an ambiguous picture of the importance of the various factors. For example from Figure 7, the maximum effect of circulation state on atmospheric CO$_2$ changes from 56 ppm to 59 ppm to 109 ppm to 0 ppm depending on whether all the pumps, the organic pump only, the solubility pump only, or none of the pumps, respectively, are acting. In contrast, the ANOVA is able to unambiguously statistically isolate the maximum effect of ocean circulation to be 12 ppm, rising to 24 ppm and 19 ppm for the interaction of circulation with the solubility or organic carbon pumps, respectively.

[45] Using the parsimonious model all the terms involving climate feedback are rejected suggesting it has a low significance. The results confirm that the organic, carbonate and solubility pumps are the dominant factors. The proportion of the variance explained by these three leading factors is greater for the log-transformed model (not shown), thus we infer that they act approximately multiplicatively in determining atmospheric CO$_2$. Together they account for 94% of the total variance of atmospheric CO$_2$ with the organic, carbonate and solubility pumps accounting for 63% (89 ppm), 6% (28 ppm) and 25% (55 ppm) of the variance, respectively. The ocean circulation is less significant accounting for 0.3% (12 ppm) of the variance but rises to 0.7% (24 ppm) of the variance of CO$_2$ when acting with the solubility pump in isolation. However, it is probable that these results underestimate the true importance of the circulation and its interaction with other factors, for reasons discussed in section 5.4.

5.1. Organic Pump

[46] Atmospheric CO$_2$ has a small (0.3% from the ANOVA) but not insignificant sensitivity (19 ppm) to circulation state when the organic pump acts alone. Unsurprisingly, when the organic pump acts in isolation, surface phosphate is not significantly different to the standard run (with all the pumps present), because it is determined by the interaction between ocean circulation state (little altered) and the imposed relaxation to zero over 6 years.

[47] However, surface ocean pCO$_2$ and thus atmospheric CO$_2$ change radically between the standard model run and the organic pump only run (Figure 8). Without the solubility pump, surface pCO$_2$ is generally significantly higher. As expected, the geographical pattern of surface pCO$_2$ is more clearly correlated with surface phosphate, because it is dominated by biological uptake. However, the average
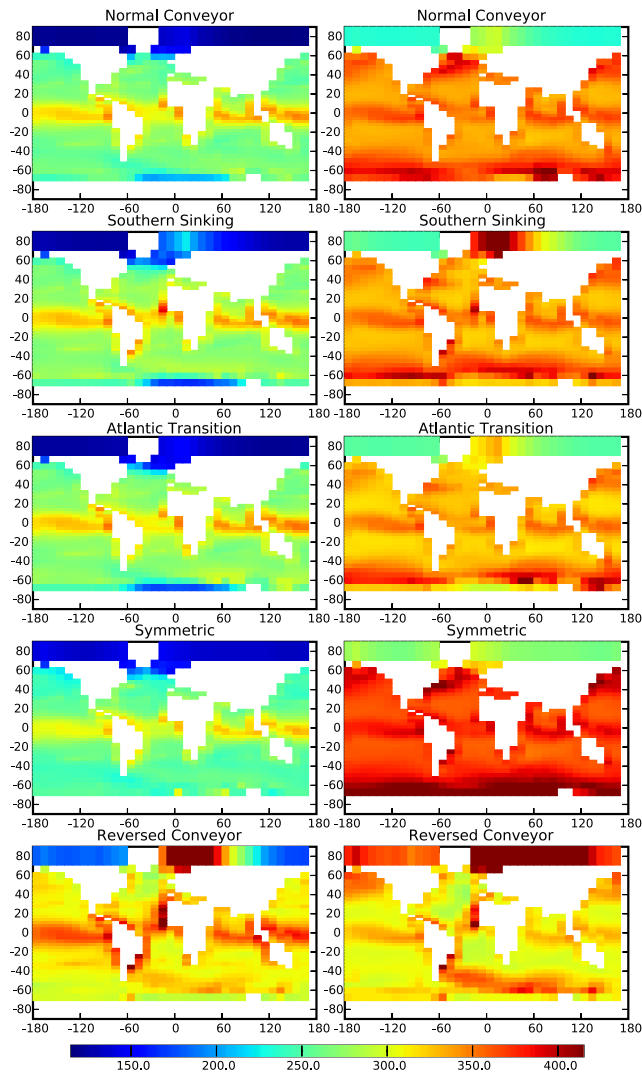
Figure 8. Annual mean ocean surface pCO$_2$ for the five circulation states using the (left) standard model and the (right) organic pump only model (see section 4.1).

concentration of surface pCO$_2$ varies significantly between the five circulation states and is not directly related to the average concentration of surface phosphate. This is especially true for the "symmetric" circulation state which has significantly higher global average surface pCO$_2$ than the others.

[48] This is not related to the conversion of surface inorganic carbon to organic carbon, which is stronger for the "symmetric state" than for the "normal conveyor." Instead in the symmetric state relative to the normal conveyor there is a significant localized change in the Southern Ocean deep convective circulation which replenishes surface waters with phosphate and DIC rich water in a timescale shorter than it is destroyed (6 years). This generates an increase in surface phosphate and DIC in the southern most latitude, especially between 0° and 60°E. This in turn increases surface ocean pCO$_2$ in this region and drives CO$_2$ into the atmosphere. Atmospheric CO$_2$

increases rapidly (90% of the gain being made over the first 100 years of the run and almost 50% in the first 10 years), driving CO$_2$ into the lower latitude surface ocean. This transport of CO$_2$ from high- to low-latitude surface waters through the atmosphere is similar to the behavior found in the box model experiments of *Toggweiler et al.* [2003a, 2003b].

[49] In addition, we note that state 4 has weaker overturning circulations in the Atlantic and Pacific than all the other circulation states (Figure 1), whereas the Southern Ocean circulation for state 4 is relatively strong (not shown). This is potentially significant; as *Toggweiler et al.* [2003a, 2003b] have argued, the relatively longer time and space scales associated with deep water traveling the length of the Atlantic (or Pacific) basins will be more effective at picking up nutrients and CO$_2$ before it is ventilated than for the Southern Ocean. This agrees with the arguments made above that the shorter timescale of the Southern Ocean circulation is crucial for the inefficiency of the organic pump in state 4.

5.2. Solubility Pump

[50] Atmospheric CO$_2$ shows greatest sensitivity (0.7% from the ANOVA, 24 ppm) to circulation state when the solubility pump acts alone: in effect a world without any plankton in the open ocean (Figure 7). The solubility pump is driven by water moving poleward, cooling, and thus absorbing more CO$_2$ from the atmosphere. Hence the strength of the pump should depend on the meridional sea surface temperature (SST) gradient and, in particular, on the temperature of the high-latitude surface waters that sink to depth and ventilate the deep ocean, setting its temperature. We find that the strength of the solubility pump is directly related to the meridional SST gradient and inversely related to the deep ocean temperature (Figure 6). Thus circulation state 5 with the weakest SST gradient also has the warmest deep ocean, the weakest solubility pump and highest CO$_2$, while circulation state 4 with the strongest SST gradient and the coldest deep ocean has the strongest solubility pump and lowest CO$_2$.

[51] There are two possible factors that could help explain these results. First, the meridional SST gradient is inversely related to the strength of the oceanic meridional circulation, which transports heat from equatorial regions to higher latitudes. Circulation state 5 has the strongest meridional overturning circulation especially in the Pacific, while state 4 has the weakest meridional overturning circulation. Secondly, the temperature of the regions of deep water formation depends on the ocean circulation state. For the "normal conveyor" (state 1), dominated by North Atlantic sinking, deep convection can occur further North than for the "reversed conveyor" (state 5) which is dominated by North Pacific sinking. Also, the climatological temperatures of the Pacific are generally warmer than the Atlantic at the same latitude. Thus water sinking to the deep in the Pacific will generally be at a higher temperature than the Atlantic leading to a weaker solubility pump.

[52] We note that there is significantly less change in the strength of the solubility pump for a reversal in the Atlantic

circulation (note the small change in atmospheric CO$_2$ going from circulation state 1 through 3 to 2, Figure 7) than for a reversal in the Pacific circulation (note the large change in atmospheric CO$_2$ going from circulation state 1 through 4 to 5). While reasons for this are not fully understood we believe that the huge size of the Pacific basin and the differing topology and climatology for the two ocean basins (as described above) as well as the greater strength of the positive Pacific cell, in state 5, than for the Atlantic circulation, in state 1, are significant in explaining the greater sensitivity of the solubility pump to changes in the Pacific circulation.

5.3. Carbonate Pump

[53] The carbonate pump tends to increase atmospheric CO$_2$ because it removes two moles of alkalinity from surface waters for each mole of carbon, thus shifting the carbonate system equilibria toward gaseous CO$_2$. There is only a weak interaction between circulation state and the carbonate pump, which was found to be insignificant in the parsimonious ANOVA. The variation that exists appears to be in a similar sense to that found for the solubility pump.

5.4. Circulation

[54] In this section we are more concerned with magnitude of the changes in atmospheric CO$_2$ due to circulation changes when all the pumps are present rather than isolating the sensitivities of atmospheric CO$_2$ due to ocean circulation and its interactions with the carbon pumps. Hence the results discussed here are taken from Figure 7 rather than from the ANOVA Table 2. Ocean circulation has a significant effect on the strength of the organic carbon and solubility pumps in the ocean. For instance the solubility pump in isolation in the "symmetric" state is more efficient than the "reversed conveyor," lowering atmospheric CO$_2$ by 109 ppm (Figure 7). However, the organic pump tends to have an antagonistic influence to the solubility pump, with the "reversed conveyor" having a 59-ppm-greater atmospheric CO$_2$ drawdown than the "symmetric" state. As a result of this antagonism between the two main carbon pumps in the ocean, the maximum net sensitivity of atmospheric CO$_2$ to circulation is reduced to 56 ppm, with the impact of the solubility pump dominating.

[55] Although we retain a modern continental configuration throughout our study, two circulation states can be identified which may have relevance to climatic events occurring during the early Cenozoic. OGCM model studies by *Bice and Marotzke* [2001, 2002] ascribe the warming event associated with the Paleocene-Eocene transition at 55.5 Ma to a switch of deep-water formation from high southern to northern latitudes. The analogue for this in our model is the change from "southern sinking" (state 2) to "reversed conveyor" (state 5) modes and we find a ≈6°C increase in deep-water temperatures associated with a switch from Southern Ocean to North Pacific dominated deep-water formation (Figure 6). This is consistent with oxygen isotope based reconstructions of the deep-water temperature increase occurring at the Paleocene-Eocene boundary [*Bains et al.*, 2000]. However, an alternative proposed time-history for early Cenozoic circulation

changes, based on the Nd paleo-circulation proxy data is that a shift in deep-water production from the Southern Ocean to the North Pacific occurred much earlier, around 65 Ma, and generally persisted in this state until the mid Eocene (40–45 Ma) [*Thomas*, 2004]. Our predicted ≈9–10°C deep-water temperatures for state 5 (reversed conveyor) are also consistent with the generally warmer (compared to modern) deep-water temperatures prevailing through the Paleocene and early Eocene [*Zachos et al.*, 2001]. Thus, although our model analysis cannot help distinguish between these two possibilities for the late Paleocene and early Eocene, not least because of our use of modern paleobathymetry, we find that the mode of circulation and source of deep-water formation exerts a powerful influence on deep ocean temperatures even in the absence of surface (climatic) warming.

[56] We predict a 38-ppm increase in pCO$_2$ associated with the transition from "southern sinking" (state 2) to "reversed conveyor" (state 5). Although this increase is rather modest, the direction of change is at least consistent with higher CO$_2$ playing a role in the relative warmth of the early Cenozoic and/or the enhanced temperatures that immediately followed the Paleocene-Eocene boundary.

[57] The implications of the organic-solubility pump antagonism for paleo climate studies is that past transitions in the mode of ocean circulation are unlikely to be an effective mechanism for driving rapid changes in CO$_2$ and radiative forcing of climate. However, we consider only the shorter-term (1–1000 year timescales) marine carbon cycle mechanisms in this study. Changes in organic carbon and carbonate burial driven by a shift in ocean circulation could potentially drive a significant long-term (>1000 years) trend in atmospheric CO$_2$ if imbalances between weathering and sedimentary burial are induced in the system, imbalances that can only be corrected on the >100,000-year timescale of continental rock weathering.

[58] A caveat to our results is that they are relevant only to ocean states with substantial advective exchange, and do not test the results of major quantitative circulation changes such as collapse to a "stagnant" state. The strength of the carbon pump is likely to depend on the global total advective (upwelling) flux, which in addition to diapycnal diffusion causes exchange of water between the surface and the depths of the ocean. Thus, although we have achieved major reorganizations of the meridional overturning circulation fields by manipulating freshwater fluxes, these states are all characterized by substantial global MOC fluxes of the order 100 Sv which is almost certainly too high because of the excessive overturning in the Southern cell. The strong Southern cell may also be masking the differences between circulation states. Therefore we have probably underestimated the full range of potential impacts of ocean circulation on the strength of the carbon pumps.

6. Conclusion

[59] Previous studies have concentrated on the relative strengths of the main oceanic pumps with one or at most two equilibrium ocean circulation states. Motivated by evidence of a number of distinctive stable ocean circulation

states in our model [*Marsh et al.*, 2004] and knowledge that the ocean circulation has been different in the past, we have considered the impact of these distinct circulation states on atmospheric CO$_2$. Future rapid climate change could cause major reorganizations of the ocean circulation, hence it is important to understand how the climate interacts with and is affected by oceanic carbon pumps and potential major ocean circulation changes. Therefore we undertook an experiment using an Earth system Model of Intermediate Complexity (GENIE-1) where all of the factors (the main oceanic pumps, the chosen stable ocean circulation states and climate change) were present and are able to interact to determine atmospheric CO$_2$.

[60] Using tests from the literature to compare GENIE-1 with other models we found that the sensitivity of atmospheric CO$_2$ to ocean pumps was generally in between that found for GCMs and box models. Real world sensitivity is also believed to fall between that found in GCMs and box models [*Toggweiler et al.*, 2003a, 2003b], although GENIE-1 may be correct for the wrong (mechanistic) reasons.

[61] A full factorial experiment design with an analysis of variance is a useful tool for unambiguously isolating the sensitivities due to the factors studied and their interactions. The factors analyzed here acted multiplicatively, the organic carbon pump explaining 63% of the variance, the solubility pump 24% and the carbonate pump 6%. The sensitivity of atmospheric CO$_2$ due to circulation alone is less significant (0.3%) although the interaction of ocean circulation with the solubility pumps increases the sensitivity (0.7%).

[62] As might be expected [*Archer et al.*, 2004], mean deep ocean temperatures were highly correlated with the strength of the solubility pump. Furthermore, the states with the weakest ocean surface temperature gradients and the warmest deep ocean temperatures had the weakest solubility pump and vice versa.

[63] The effect of changes in the mode of circulation when all the oceanic pumps were present (56 ppm) was reduced relative to the effect of changes in circulation when the solubility pump was acting in isolation (109 ppm). This was partially due to the organic and solubility pumps having opposing effects under ocean circulation changes. For the "symmetric" and "reversed conveyor" states, marine biological production and the particulate organic carbon ameliorates the impact on atmospheric CO$_2$ that would occur due to a change in the effectiveness of the solubility pump alone.

[64] The lack of sensitivity of atmospheric CO$_2$ to changes in ocean circulation is also probably due to the strength of the meridional overturning circulation not varying greatly across the different ocean circulation states considered. Much of the thermohaline circulation is controlled by the strength of diapycnal mixing, especially in the Southern Ocean and the North Pacific [*Saenko and Merryfield*, 2005]. The strength of diapycnal mixing depends on the amount of turbulent kinetic energy (TKE) provided by winds and tides. We kept diapycnal diffusivity constant throughout this study. Recent evidence suggests that both sources of TKE have varied widely, for example in the recent past due to changes in sea level and

tides [*Arbic et al.*, 2004]. A follow-on study is considering the effects of changing the ocean circulation strength significantly in isolation from changes to the "structure" of the circulation.

[65] We found that when the organic pump was operating in isolation, the changes in ocean circulation had the largest effect on atmospheric CO$_2$ when the timescale for replenishment of nutrients in the surface Southern Ocean was decreased relative to surface nutrient destruction and when the ocean circulations in both the Atlantic and the Pacific weakened. In agreement with *Toggweiler et al.* [2003a, 2003b], we find that the shorter timescale for ventilation of the Southern Ocean versus the Atlantic and Pacific is important in determining the strength of the organic pump. Furthermore, the circulation mode in the Pacific rather than Atlantic was in general of greater significance for the organic and solubility pumps and thus for atmospheric CO$_2$. We therefore suggest that past and future changes in the oceanic circulation in the Pacific may be more significant for atmospheric CO$_2$ concentrations and climate change than those in the Atlantic.

References

Andersson, J., J. Wijsman, P. Herman, J. Middelburg, K. Soetaert, and C. Heip (2004), Respiration patterns in the deep ocean, *Geophys. Res. Lett.*, *31*, L03304, doi:10.1029/2003GL018756.

Annan, J. D., J. C. Hargreaves, N. R. Edwards, and R. Marsh (2004), Parameter estimation in an intermediate complexity earth system model using an ensemble Kalman filter, *Ocean Modell.*, *8*, 135–154, doi:101016/j.ocemod.203.12.004.

Arbic, B. K., D. R. MacAyeal, J. X. Mitrovica, and G. A. Milne (2004), Ocean tides and Heinrich events, *Nature*, *432*, 460.

Archer, D. E., H. Kheshgi, and E. Maier-Reimer (1998), Dynamics of fossil fuel CO$_2$ neutralization by marine CaCO$_3$, *Global Biogeochem. Cycles*, *12*(2), 259–276.

Archer, D. E., G. Eshel, A. Winguth, W. Broecker, R. Pierrehumbert, M. Tobis, and R. Jacob (2000a), Atmospheric *p*CO$_2$ sensitivity to the biological pump in the ocean, *Global Biogeochem. Cycles*, *14*(4), 1219–1230.

Archer, D. E., A. Winguth, D. Lea, and N. Mahowald (2000b), What caused the glacial/interglacial pCO$_2$ cycles?, *Rev. Geophys.*, *38*, 159–189.

Archer, D. E., P. Martin, B. Buffett, V. Brovkin, S. Rahmstorf, and A. Ganopolski (2004), The importance of ocean temperature to global biogeochemistry, *Earth Planet. Sci. Lett.*, *222*, 333–348.

Bains, S., R. D. Norris, R. M. Corfield, and K. L. Faul (2000), Termination of global warmth in the Paleocene/Eocene boundary through productivity feedback, *Nature*, *407*, 171–174.

Bice, K. L., and J. Marotzke (2001), Numerical evidence against reversed thermohaline circulation in the warm Paleocene/Eocene ocean, *J. Geophys. Res.*, *106*, 11,529–11,542.

Bice, K. L., and J. Marotzke (2002), Could changing ocean circulation have destabilized methane hydrate at the Paleocene/Eocene boundary?, *Paleoceanography*, *17*(2), 1018, doi:10.1029/2001PA000678.

Bopp, L., P. Monfray, O. Aumont, J.-L. Dufresne, H. LeTreut, G. Madec, L. Terray, and J. Orr (2001), Potential impact of climate change on marine export production, *Global Biogeochem. Cycles*, *15*(1), 81–99.

Bopp, L., O. Aumont, S. Belviso, and P. Monfray (2003), Potential impact of climate change on marine dimethyl sulfide emissions, *Tellus, Ser. B*, *55*, 11–22, doi:10.1034/j.1600-0889.2003.042.x.

Broecker, W., and T.-H. Peng (1986), What caused the glacial to interglacial atmospheric CO$_2$ change?, *Radiocarbon*, *28*, 309–327.

Broecker, W., J. Lynch-Stieglitz, D. E. Archer, M. Hofmann, E. Maier-Reimer, O. Marchal, T. Stocker, and N. Gruber (1999), How strong is the Harvardton-Bear constraint?, *Global Biogeochem. Cycles*, *13*(4), 817–820.

Davies, O. L., and P. L. Goldsmith (1972), *Statistical Methods in Research and Production*, 4th ed., Longman, New York.

Edwards, N. R., and R. Marsh (2005), Uncertainties due to transport-parameter sensitivity in an efficient 3-D ocean-climate model, *Clim. Dyn.*, *24*, 415–433.

Gnanadesikan, A., R. D. Slater, N. Gruber, and J. L. Sarmiento (2002), Oceanic vertical exchange and new production: A comparison between models and observations, *Deep Sea Res., Part II*, *49*, 363–401.

Grafen, A., and R. Hails (2002), *Modern Statistics for the Life Sciences*, Oxford Univ. Press, New York.

Hargreaves, J. C., J. D. Annan, N. R. Edwards, and R. Marsh (2004), An efficient climate forecasting method using an intermediate complexity Earth System Model and the ensemble Kalman filter, *Clim. Dyn.*, *23*, 745–760, doi:10.1007/s00382-004-0471-4.

Heinze, C., E. Maier-Reimer, A. M. E. Winguth, and D. E. Archer (1999), A global oceanic sediment model for long term climate studies, *Global Biogeochem. Cycles*, *13*(1), 221–250.

Hosoe, T. (2004), Stability of the global thermohaline circulation in an intermediate complexity ocean model, Ph.D. thesis, School of Ocean and Earth Sci., Univ. of Southampton, Southampton, UK.

Joos, F., G.-K. Plattner, T. F. Stocker, O. Marchal, and A. Schmittner (1999), Global warming and marine carbon cycle feedbacks an future atmospheric CO$_2$, *Science*, *284*, 464–467.

Knox, F., and M. McElroy (1984), Change in atmospheric CO$_2$: Influence of marine biota at high latitude, *J. Geophys. Res.*, *89*, 4629–4637.

Maier-Reimer, E. (1993), Geochemical cycles in an ocean general circulation model: Preindustrial tracer distributions, *Global Biogeochem. Cycles*, *7*(3), 645–677.

Marsh, R., A. Yool, T. M. Lenton, M. Y. Gulamali, N. R. Edwards, J. G. Shepherd, M. Krznaric, S. Newhouse, and S. J. Cox (2004), Bistability of the thermohaline circulation identified through comprehensive 2-parameter sweeps of an efficient climate model, *Clim. Dyn.*, *23*, 761–777, doi:10.1007/s00382-004-0474-1.

Martin, J. H., G. A. Knauer, D. M. Karl, and W. W. Broenkow (1987), VERTEX: Carbon cycling in the northwest Pacific, *Deep Sea Res.*, *34*, 267–285.

Orr, J. C., et al. (2001), Estimates of athropogenic carbon uptake from four three-dimensional global ocean models, *Global Biogeochem. Cycles*, *15*(1), 43–60.

Plattner, G.-K., F. Joos, T. F. Stocker, and O. Marchal (2001), Feedback mechanisms and sensitivities of ocean carbon uptake under global warming, *Tellus, Ser. B*, *53*, 564–592.

Redfield, A. C., B. H. Ketchum, and F. A. Richards (1963), The influence of organisms in the composition of sea water, in *The Sea*, vol. 32, edited by N. M. Hill, pp. 26–77, Wiley-Intersci., Hoboken, N. J.

Ridgwell, A. J. (2001), Glacial-interglacial perturbations in the global carbon cycle, Ph.D. thesis, Univ. of East Anglia at Norwich, Norwich, UK.

Ridgwell, A. J., A. J. Watson, and D. E. Archer (2002), Modelling the response of the oceanic Si inventory to perturbation and consequences for atmospheric CO$_2$, *Global Biogeochem. Cycles*, *16*(4), 1071, doi:10.1029/2002GB001877.

Saenko, O. A., and W. J. Merryfield (2005), On the effect of topographically enhanced mixing on the global ocean circulation, *J. Phys. Oceanogr.*, *35*, 826–834.

Sarmiento, J. L., and C. Le Quere (1996), Oceanic carbon dioxide uptake in a model of century-scale global warming, *Science*, *274*, 1346–1349.

Sarmiento, J. L., and J. R. Toggweiler (1984), A new model for the role of the oceans in determining atmospheric pCO$_2$, *Nature*, *308*, 621–624.

Sarmiento, J. L., T. M. C. Hughes, R. J. Stouffer, and S. Manabe (1998), Simulated response of the ocean carbon cycle to anthropogenic climate warming, *Nature*, *393*, 245–249.

Sarmiento, J. L., J. Dunne, A. Gnanadesikan, R. M. Key, K. Matsumoto, and R. Slater (2002), A new estimate of the CaCO$_3$ to organic carbon export ratio, *Global Biogeochem. Cycles*, *16*(4), 1107, doi:10.1029/2002GB001919.

Siegenhaler, U., and T. Wenk (1984), Rapid atmospheric CO$_2$ variations and ocean circulation, *Nature*, *308*, 624–626.

Six, K. D., and E. Maier-Reimer (1996), Effects of plankton dynamics on seasonal carbon fluxes in an ocean general circulation model, *Global Biogeochem. Cycles*, *10*(4), 559–583.

Thomas, D. J. (2004), Evidence for deep-water production in the North Pacific Ocean during the early Cenozoic warm interval, *Nature*, *430*, 65–68.

Toggweiler, J. R., A. Gnanadesikan, S. Carson, R. Murnane, and J. L. Sarmiento (2003a), Representation of the carbon cycle in box models and GCMs: 1. Solubility pump, *Global Biogeochem. Cycles*, *17*(1), 1026, doi:10.1029/2001GB001401.

Toggweiler, J. R., R. Murnane, S. Carson, A. Gnanadesikan, and J. L. Sarmiento (2003b), Representation of the carbon cycle in box models and GCMs: 2. Organic pump, *Global Biogeochem. Cycles*, *17*(1), 1027, doi:10.1029/2001GB001841.

Volk, T., and M. I. Hoffert (1985), Ocean carbon pumps: Analysis of relative strengths and efficiencies in ocean driven atmospheric pCO$_2$ changes, in *Carbon Dioxide and the Carbon Cycle, Archean to Present*, *Geophys. Monogr. Ser.*, vol. 32, edited by E. T. Sundquist and W. S. Broecker, pp. 99–110, AGU, Washington, D. C.

Watson, A. J. (2001), Iron limitation in the oceans, in *The Biogeochemistry of Iron in Seawater*, edited by D. R. Turner and K. A. Hunter, pp. 9–39, John Wiley, Hoboken, N. J.

Yamanaka, Y., and E. Tajika (1996), The role of the vertical fluxes of particulate organic matter and calcite in the oceanic carbon cycle: Studies using an ocean biogeochemical general circulation model, *Global Biogeochem. Cycles*, *10*(2), 361–382.

Zachos, J. C., M. Pagani, L. C. Sloan, E. Thomas, and K. Billups (2001), Trends, rhythms and aberations in global climate 65Ma to present, *Science*, *292*, 686–693.

————————————

D. R. Cameron, Centre for Ecology and Hydrology, Bush Estate, Penicuik, EH26 0QB, UK. (dcam@ceh.ac.uk)

T. M. Lenton, School of Environmental Sciences, University of East Anglia, Norwich, NR4 7TJ, UK. (t.lenton@uea.ac.uk)

R. Marsh, J. G. Shepherd, and A. Yool, National Oceanography Centre, European Way, Southampton, SO14 3ZH, UK. (rma@noc.soton.ac.uk; j.g.shepherd@noc.soton.ac.uk; axy@noc.soton.ac.uk)

A. J. Ridgwell, Department of Earth and Ocean Sciences, University of British Columbia, 6339 Stores Road, Vancouver, BC, Canada V6T 1Z4. (aridgwell@eos.ubc.ca)